Structural and Multidisciplinary Optimization (2021) 64:1983–1995
https://doi.org/10.1007/s00158-021-02959-3

RESEARCH PAPER

Multiscale design of functionally graded cellular structures for additive manufacturing using level-set descriptions

Cong Hong Phong Nguyen[1] · Young Choi[2]

Received: 9 July 2020 / Revised: 15 March 2021 / Accepted: 17 May 2021 / Published online: 3 June 2021

Abstract

The emergence of additive manufacturing (AM) has enabled the design of complex structures with high performance, such as functionally graded cellular structures (FGCSs). Concurrent topology optimization is commonly utilized for designing FGCSs; however, this approach suffers from an extremely high computational cost due to the complexity of the design problem. Recently, level-set-based methods, which rely on the implicit-based modeling technique, have gained increased attention and been considered as an efficient design tool for structures fabricated with AM. In this work, a multiscale structural optimization method for FGCS design utilizing level-set descriptions is proposed. Contrary to the well-known level-set topology optimization, in this approach, the shape is represented and parameterized with implicit functions, and the optimization process is performed to find the optimal parameters. The proposed method can replace topology optimization for microscale structural optimization within the multiscale structural design with reduced computation cost and comparable optimally designed results. Moreover, the unique behaviors of pre-selected cellular structures could be maintained during the optimization process by proper parametric constraints. The proposed design approach was validated through two design examples, both of which demonstrate remarkable structural performance enhancements in comparison with the single-scale design approach. Furthermore, two three-dimensional design examples, commonly found in automotive and aerospace industries, further prove the applicability of the proposed method in practice.

Keywords Multiscale structural optimization · Level-set description · Implicit modeling · Functionally graded cellular structures · Design for additive manufacturing

1 Introduction

Cellular structures, made from a series of connecting struts and plates, are well known for their multi-functionality and high strength-to-weight ratios. Recent advances in additive manufacturing (AM) have improved fabrication capabilities of such complex shapes including cellular structures. Multiscale structural optimization is commonly utilized to design cellular structures as it allows the design space, including both macroscale and microscale, to be fully explored. Recently, the level-set-description-based method has been considered as a promising candidate for replacing expensive topology optimization–based methods in multiscale structural design (Noël and Duysinx 2016). In comparison with conventional topology optimization, the level-set-based method is well suited with AM as well as posing advantages of being less complicated and easier for post-processing since it utilizes implicit functions to represent shapes (Liu et al. 2018b).

In this work, a multiscale, level-set-description-based method for designing functionally graded cellular structures (FGCSs), a typical type of cellular structure, is proposed. In particular, the microscale structural optimization problem is solved using the level-set-description-based method, which features a low-cost and effective computation process compared to conventional topology optimization approaches. Moreover, unique behaviors of cellular structures (such as negative Poisson's ratio) could be pre-determined and

Responsible Editor: Xu Guo

✉ Young Choi
yychoi@cau.ac.kr

[1] Department of Mechanical Engineering, Graduate School, Chung-Ang University, 84 Heukseok-ro, Dongjak-gu, Seoul 06974, South Korea

[2] School of Mechanical Engineering, College of Engineering, Chung-Ang University, Bldg 310, Room 538, 84 Heukseok-ro, Dongjak-gu, Seoul 06974, South Korea

maintained during the optimization with proper constraints. Due to the customization of each unit cell, the proposed method could enhance structural performances in comparison with other single-scale design approaches for FGCSs. In addition, smooth interconnectivity between adjacent cellular unit cells is ensured by applying implicit blending in the structure synthesis process. Finally, a robust solution for fabrication of optimally designed structures is affordable due to the application of implicit-based modeling for post-processing.

The rest of the paper is organized as follows. Section 2 provides a summary of related works. Section 3 introduces the microstructure representation utilizing level-set description and implicit blending. Section 4 presents the level-set-description-based multiscale structural optimization for FGCS design. Experimental studies are discussed in Section 5 to validate the proposed design approach in practice. Conclusions and future works are given in Section 6.

2 Literature review

FGCS is a specific type of cellular structure whereby the distribution of material is locally designed to serve specific functionalities. The most straightforward approach for designing FGCSs is populating the domain with cellular structures, usually truss-element-based structures, and performing a size optimization. Some notable works following this approach include relative density mapping reported by Alzahrani et al. (2015) and the bi-directional evolutionary structural optimization (BESO)–based approach reported by Tang et al. (2015). Because truss-element-based approaches are limited in dealing with complex microstructure and multi-physics problems, the volume-element-based approach is adopted more often. In this approach, either single-scale or multiscale structural optimization can be applied. Single-scale optimization methods often require pre-analyzed constitutive interpolation models of cellular structures and it is referred to as the homogenization-based approach (Li et al. 2018; Li et al. 2020; Cheng et al. 2017; Zhang et al. 2015). Moreover, applying the volume-element-based approach allows one to reflect the material properties of AM parts (Nguyen et al. 2019), perform multi-physics design (Tang and Zhao 2018), and even customize the cellular unit cell for better structural performance. The unit cell customization issue is referred to as concurrent structural optimization. In concurrent structural optimization, the multiscale design problem is separated into macroscale and microscale problems, with homogenization typically utilized to connect the two scales. Within the finite element analysis (FEA) framework, this approach is known as the finite element square (FE^2) method, and it is used to deal with the nonlinearity of the multiscale design problem (Xia 2016c). The structural design at both scales can be performed at different levels including size, shape, and topology optimization. Among these, topology optimization is applied most often due to its high level of design freedom and flexibility. Wu et al. (2019) proposed a design method for graded lattice structures by applying the approximation of reduced substructure with a penalization model. In contrast to the density-based topology optimization, Sivapuram et al. (2016) proposed a simultaneous material and structural design by applying a multiscale topology optimization using the level-set method. In addition, the level-set method was applied in the concurrent design of FGCSs for additive manufacturing (Fu et al. 2019; Wang et al. 2017; Wang et al. 2018). Although significant efforts have been made to reduce the required computational cost, it is still the main disadvantage of designing cellular structures relying on coupled multiscale topology optimization.

Implicit modeling is a shape representation method where the boundary of a structure is not determined explicitly but rather via the "zero-set" of a level-set function (Velho et al. 2002). Due to breakthroughs in AM, this kind of volume-based representation scheme is preferable to surface-based representation, especially for heterogeneous objects. Several advantages of the implicit modeling technique such as the function-based slicing process proposed by Song et al. (2018) have been demonstrated. Additionally, Steuben et al. (2016) proposed a method for designing functionally tailored structures using implicit slicing. The application of implicit representation in designing cellular structures was then generalized by Fryazinov et al. (2013) as the multiscale space-variant function representation.

Level-set-based methods play a crucial role in structural optimization with smooth designs and a high level of satisfaction (Allaire et al. 2004; Wang et al. 2003). Further, the level-set topology optimization provides post-processing benefits such as structure synthesis from the optimal design result or direct structural fabrication, which are discussed in detail in Liu et al. (2018b). Moreover, the level-set-based method can be applied for parameterized shape optimization. This approach is referred to as the application of level-set descriptions (Noël and Duysinx 2016) and is distinct from the well-known level-set topology optimization. Due to its compactness and effectiveness in structural optimization, the design process utilizing level-set descriptions has been receiving increased attention and therefore has been used in the present study.

3 Level-set description approach for micro-cellular structure modeling

3.1 Level-set descriptions

The level-set method is introduced as a method to track the interface movement in a continuous domain within physics problems. In shape modeling, the boundary of a structure is defined as the "zero-set" of an implicit function:

$$\begin{cases} \Phi(\boldsymbol{x},\boldsymbol{s}) \geq 0\ \boldsymbol{x} \in \Omega \\ \Phi(\boldsymbol{x},\boldsymbol{s}) = 0\ \boldsymbol{x} \in \Gamma \\ \Phi(\boldsymbol{x},\boldsymbol{s}) < 0\ \boldsymbol{x} \notin \Omega \end{cases}, \tag{1}$$

where Φ is the level-set description at $\boldsymbol{x}(x_1, x_2, \ldots x_i)$ which is the coordinate of the sampling point in n-dimensional space, $\boldsymbol{s}(s_1, s_2, \ldots, s_j)$ is the parameter set that defines the structural level-set function, Ω is the domain inside the structure, and Γ is the structure boundary.

As mentioned earlier, the boundary of the structure will be determined by extracting the zero-set, which are iso-contours in two-dimensional (2D) cases and iso-surfaces in three-dimensional (3D) cases, of the given level-set function. This work requires evaluation of the level-set function over the sampling domain, resulting in an extremely cumbersome computation. However, due to the current development of the graphics processing unit (GPU), level-set descriptions can be evaluated faster by parallel computing, which considerably reduces the computational cost and makes this design approach more practical.

3.2 Joint-based representation approach for micro-cellular structure

Before further discussion, it is worth noting that in this work, 2D cellular structures are focused for simplification although this approach is also applicable for 3D cellular structures. In particular, a 2D wall-based cellular structure (Fig. 1a) is constructed by connecting "joints" by "walls" (Fig. 1b); thus, the most trivial way to represent a cellular structure is implicitly uniting cellular walls. Therefore, at a given sampling point, the level-set description of a cellular structure is determined as:

$$C(x) = U(w_i(x)) \mid i = 1 \ldots M, \tag{2}$$

where $C(x)$ and $w_i(x)$ are level-set descriptions of the cellular structure and cellular walls, respectively, at the sampling point x and M is the number of walls. The implicit union operation is simply a Boolean union, where:

$$U = \max(f_i). \tag{3}$$

The level-set description of a given wall $w_i(x)$ is calculated as:

$$w_i(x) = -\left[d(x, wc_i) - \frac{t_i}{2}\right], \tag{4}$$

where $d(x, wc_i)$ is the distance from sampling point x to the centerline of the wall wc_i, and t_i is the thickness of the wall. Unfortunately, modeling cellular structures using this approach poses several potential issues including stress concentration due to sharp corners and design freedom limitation due to the lack of design variables. Therefore, an alternative approach utilizing blending operators is proposed to overcome these issues.

The level-set description of a blended joint between cellular walls could then be calculated via the Kreisselmeier-Steinhauser (KS) function:

$$C(w_1(x), w_2(x), \ldots, w_M(x), \beta) = KS(w_i(x), \beta) = \frac{1}{\beta} \ln\left(\sum_{i=1}^{n} e^{-\beta w_i(x)}\right), \tag{5}$$

where β is the blending parameter. The variation of β determines the smoothness of the resulting cellular structure. When β is extremely large, the KS function is similar to the conventional implicit Boolean operation. Figure 2 shows an example of a hexagonal honeycomb structure with various blending parameters.

Utilizing the KS blending function is beneficial with controllable local smoothness; however, applying it as a global function limits the design freedom in structural optimization. In this work, a joint-based modeling approach motivated by the work from Panetta et al. (2017) is applied. Typically, the level-set description of cellular structures is a KS blending of cellular joints which is KS blending of cellular walls:

$$C_B = KS\left(N_j(x), \beta\right), \tag{6}$$

$$N_j(x) = KS\left(w_i(x), \beta_j\right), \tag{7}$$

where $N_j(x)$ is joint j, which is formed by the cellular wall $w_i(x)$; β is the global blending parameter; and β_j are local blending parameters that are assigned to joint j. Figure 3 illustrates the local smoothness control of the joint. In addition, one cellular wall $w_i(x)$ could be shared by several joints $N_j(x)$, and the smoothness between those joints is controlled by the global blending parameter β.

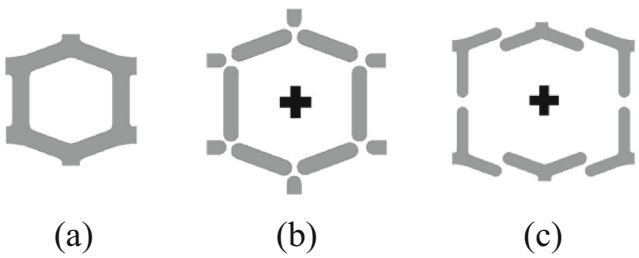

Fig. 1 (**a**) Honeycomb structure. (**b**) Conventional wall-based modeling approach. (**c**) Joint-based approach

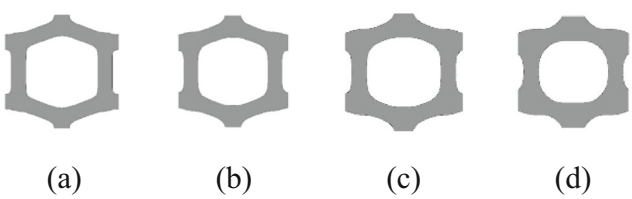

Fig. 2 Hexagonal honeycomb structure with varied blending parameters. (**a**) $\beta = 24$. (**b**) $\beta = 12$. (**c**) $\beta = 8$. (**d**) $\beta = 4$

Fig. 3 Local control of the joint-based design approach. (**a**) Joint's blending parameter = 24. (**b**) Joint's blending parameter = 3

3.3 Conversion from geometric models to mechanical models using density approach

It is required to convert the geometric model to mechanical model, i.e., finite element model, for structural optimization. Herein, this is done using the density-based approach.

Using the density-based approach, the elastic modulus of an element e is determined as:

$$E_e = E\rho_e, \tag{8}$$

where E is the elastic modulus of the full solid element, and ρ_e is the element relative density. In 2D case, ρ_e is calculated as:

$$\rho_e = \frac{A_e}{A}, \tag{9}$$

where A_e is the element's actual area, and A is the element's area when $\rho_e = 1$.

A_e is calculated using the marching square algorithm by using level-set description corners of the element. Figure 4 illustrates the conversion from the geometric model to the mechanical model for various cellular structures.

4 Multiscale design of functionally graded cellular structures

In this work, a decoupled multiscale scheme is employed to replace the expensive fully coupled scheme to which the FE^2 method is applied (Xia 2016b). Figure 5 illustrates the overall workflow of the proposed multiscale structural optimization

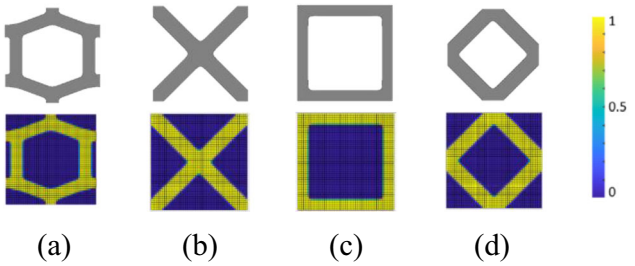

Fig. 4 Illustration of the conversion from geometric (top) to mechanical model (bottom) conversion for various structures. (**a**) Hexagonal honeycomb. (**b**) Diagonal. (**c**) Cube. (**d**) Diamond

for the FGCS design approach. In the first stage, the homogenization-based design method is employed to optimize the density distribution of the macroscale design domain which has been tessellated into multiple representative volume elements (RVEs) (Nguyen et al. 2019). In the second stage, the microstructure of each RVE is optimized with the proposed level-set-description-based method.

4.1 Macroscale structural optimization

Given a tessellated and populated with predefined cellular structure design domain, the macroscale structural optimization problem is formulated as in Eq. 10. The objective of the macroscale structural optimization is to find the optimal density distribution of FGCSs; thus, the result of the optimization is not the extreme "0" and "1" as that of conventional topology optimization.

$$\begin{aligned}
&\min_{\boldsymbol{\rho}} \mathrm{c}(\boldsymbol{u}) = \boldsymbol{F}^{\boldsymbol{T}}\boldsymbol{u}; \{\, \boldsymbol{\rho}(\rho_1, \ldots, \rho_N) \,\} \\
&\text{s.t}: \\
&\boldsymbol{K}\boldsymbol{u} = \boldsymbol{F}; \\
&\boldsymbol{K} = \bigwedge_{e=1}^{N} \boldsymbol{K}_e; \boldsymbol{K}_e = \boldsymbol{K}_e\left(\boldsymbol{C}_e\left(\rho_e\right)\right); \\
&\sum_{e=1}^{n} V_e\rho_e \le V_{target} \\
&0 \le \rho_{low} \le \rho_e \le \rho_{high} \le 1;
\end{aligned} \tag{10}$$

In the problem described in Eq. 10, the design objective is to find the optimal relative density $\boldsymbol{\rho}$ of N number of RVEs to minimize the structural total compliance c under a given loading $\boldsymbol{F}$. Meanwhile, $\boldsymbol{u}$ is the nodal displacement vector, and $\boldsymbol{K}$ is the global stiffness matrix. $\boldsymbol{K}$ is assembled from element stiffness matrices $\boldsymbol{K}_e$, which are derived from the pre-analyzed scaling laws $\boldsymbol{C}_e(\rho_e)$ assigned for each RVE. The volume constraint is represented by V_{target}. This problem can be solved using a gradient-based approach. The sensitivity of the objective function, with respect to the change of a density variable ρ_e, can be computed as in Eq. 11 since it is a self-adjoint problem:

$$\frac{\partial c}{\partial \rho_e} = -\boldsymbol{u}_e^T \frac{\partial \boldsymbol{K}_e}{\partial \rho_e}\boldsymbol{u}_e, \tag{11}$$

and the derivative of $\boldsymbol{K}_e$ is calculated from the finite element integration equation:

$$\frac{\partial \boldsymbol{K}_e}{\partial \rho_e} = \int_V \boldsymbol{B}_e^T \frac{\partial \boldsymbol{C}_e(\rho_e)}{\partial \rho_e}\boldsymbol{B}_e dV_e. \tag{12}$$

4.2 Microscale structural optimization

In the microscale structural optimization problem, a 2D microscale cellular structure with P joints and Q walls is given. Blending parameters β_i are assigned for each joint, and wall

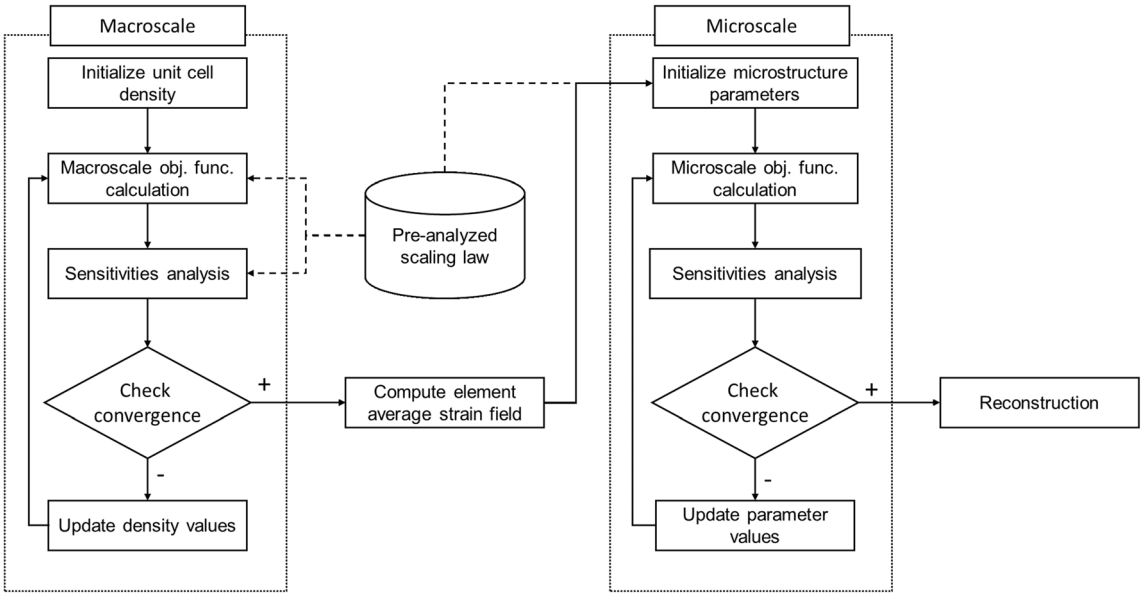

Fig. 5 Overall design workflow of the multiscale structural optimization

thickness parameters t_j are assigned to each wall. The objective of the microscale structural optimization is to maximize the microscale material stiffness a prescribed average strain ε_0 calculated from the macroscale design result (Xia 2016b). The microscale structural optimization problem could be formulated as follows:

$$\begin{aligned} &\max_{s} \; J = \boldsymbol{v}^T \boldsymbol{K}_m \boldsymbol{v}; \boldsymbol{s} = \{\, \boldsymbol{t}(t_1, \ldots, t_P); \boldsymbol{\beta}(\beta_1, \ldots, \beta_Q) \,\} \\ &s.t: \\ &\overline{\varepsilon} = \boldsymbol{\varepsilon_0} \\ &V(\boldsymbol{s}) = V_{target} \\ &0 < t_{min} \le t_i \le t_{max}; i = 1 \ldots P \\ &1 < \beta_{min} \le \beta_j \le \beta_{max}; j = 1 \ldots Q \end{aligned} \tag{13}$$

In Eq. 13, J is the microscale material stiffness, determined by the twice of strain energy which causes the microscale displacement $\boldsymbol{v}$ under a prescribed macroscale strain ε_0. Also, $\boldsymbol{K}_m$ is the global stiffness matrix of the microscale cellular structure. Additionally, the volume constraint is treated as an equality constraint since the microstructure should maintain its predefined volume during the optimization. Further, the periodic boundary condition (PBC) that requires an identical mesh grid is naturally satisfied by the level-set-description-based approach.

The optimization problem is solved using the gradient-based approach. In this work, a semi-analytical approach is applied to calculate the sensitivities. From the literature, the problem as formulated in Eq. 13 is self-adjoint, so the sensitivities of the objective function are:

$$\frac{\partial J}{\partial s} = \boldsymbol{v}^T \frac{\partial \boldsymbol{K}_m}{\partial s} \boldsymbol{v}. \tag{14}$$

The microscale global stiffness sensitivities are assembled from element stiffness sensitivities of R number of microscale material elements:

$$\frac{\partial \boldsymbol{K}_m}{\partial s} = \bigwedge_{me=1}^{R} \frac{\partial \boldsymbol{K}_{me}}{\partial s}. \tag{15}$$

Here, the microscale element stiffness sensitivities are calculated as a function of microscale element density (η_{em}) derivatives:

$$\frac{\partial \boldsymbol{K}_{em}}{\partial s} = E \frac{\partial \eta_{em}}{\partial s} \boldsymbol{k}_{m0}, \tag{16}$$

where $\boldsymbol{k}_{m0}$ is the microscale element stiffness matrix when $E = 1$.

The derivatives of the microscale element densities can be derived using the central finite difference scheme:

$$\frac{\partial \eta_{me}}{\partial s} = \frac{\eta_{me}(s + \Delta s) - \eta_{me}(s - \Delta s)}{2\Delta s}, \tag{17}$$

where Δs is an extremely small number. Specifically, in this work, Δs is set as 10^{-6}.

5 Experimental studies

In this section, the proposed design method is validated via experimental studies with numerical simulation. MATLAB programming language was utilized for implementation. In addition, the method of moving asymptotes (MMA) algorithm (Svanberg 1987) was used to solve the aforementioned optimization problems. All simulations were conducted on a

laboratory computer with an AMD®Ryzen Threadripper CPU @3.50 GHz, 12 cores, 20 threads, and 32.0 GB RAM.

5.1 Single unit cell optimization

In this section, a comparison between the proposed method and topology optimization in cellular material design is conducted. Six types of cellular unit cell (Fig. 6) with multiple prescribed strain values as in Table 1 were tested and compared with the topology optimization result. The unit cell resolution was selected as 50 × 50 unit length, the wall thickness constraint is set as 2~20 unit length, and the blending constraint is 1.5~24. The benchmarking was conducted under two criteria: (1) the value of the objective function, which is the stiffness of the designed unit cell, and (2) time consumption. Topology optimization was applied in this experiment based on the guidance of Xia (2016a).

Figure 7 depicts single unit cell optimization results, and Tables 2 and 3 show the summary of objective function value and time consumption of the optimization process. Moreover, the convergence history of the best design configurations (cube, diamond, cube + diagonal, and cube, respectively) and topology optimization for four strain cases is shown in Fig. 8. In terms of optimality achievement, the proposed method shows a dependency on pre-selected unit cell geometry. For the first three types of unit cell, the cube, diagonal, and diamond, while the cube shape behaves better in cases more oriented to uniaxial strain (cases 1, 3, and 4), the diagonal and diamond shapes show better performance in the shear strain–oriented case which is case 2. The last three types of unit cell, the cube and diagonal combined, the cube and diamond combined, and the hexagon honeycomb, seem to be more balanced with most strain cases.

In comparison with the topology optimization approach, in terms of optimality achievement, the proposed approach is comparable. In all strain cases, the best unit cell designed by the proposed method could achieve an average of 91.79% of the optimal values derived by topology optimization. From the time consumption comparison result in Table 3, the level-set description approach method shows better computation efficiency in comparison with topology optimization. From the comparison results, it was found that the proposed method could be utilized as a replacement for topology optimization in microscale structural optimization, especially within the context of multiscale structural optimization.

Table 1 Prescribed strain values in the benchmarking of a single unit cell optimization problem

No.	Prescribe strain value	Note
1	[1.00;0.00;0.00]	Uniaxial strain
2	[0.00;0.00;1.00]	Shear strain
3	[0.71;0.71;0.00]	Two-directional uniaxial strain
4	[0.83;0.14;0.54]	General strain

5.2 Cellular three-point bending beam design

Three-point bending beam design problems and its variations are commonly considered for validations in structural optimization. In this design problem, a beam with dimensions of 150 × 50 mm under the loading condition, as described in Fig. 9(a), was designed with the cubic unit cell, shown in Fig. 9(b).

For the macroscale structural optimization, pre-analyzed scaling laws of cubic unit cell as shown in Fig. 9(c) were used, with fit rates of at least 95%. Additionally, the fitting coefficients are provided in Table 4. Here, C^* denotes the effective elastic constant of the microstructure, whereas C denotes the elastic constant of the microstructure when its relative density $\rho = 1$. The relative density range of RVEs is set to be in the range of 0.3–0.8, and the volume fraction constraint is 0.55, with unit cell size of 5 mm. For the microscale structural optimization, a 50 × 50 uniform grid was used. The wall thickness and blending parameter ranged from 0.15~2.0 (mm) and 2~12, respectively, based on experimental results.

Figure 10 illustrates the design results. The proposed design approach was benchmarked with a non-optimized microstructure FGCS. Figure 11 shows the benchmarking of two designs with FEA results. The proposed method derived a structure designed with superior structural stiffness, with a compliance reduction of 22.8% (from 26.675 to 20.586), compared to the non-optimized microstructure. This result can be explained visually as the structure designed by the proposed approach varies the unit cell shape in a way that follows both the density and orientation of the stress stream (Fig. 12).

Fig. 6 Cellular unit cell considered in the benchmarking of a single unit cell optimization problem. (**a**) Cube. (**b**) Diagonal. (**c**) Diamond. (**d**) Cube + diagonal. (**e**) Cube + diamond. (**f**) Hexagon honeycomb

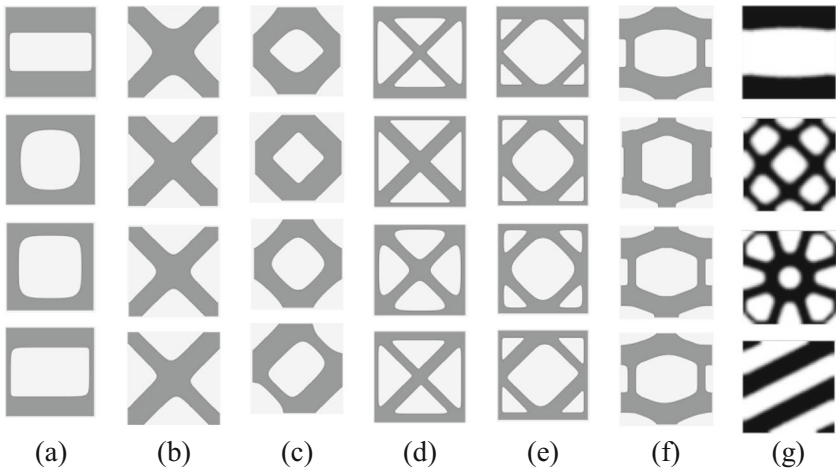

Fig. 7 Single unit cell optimization result of four strain cases arranged from top to bottom. (**a**) Cube. (**b**) Diagonal. (**c**) Diamond. (**d**) Cube + diagonal. (**e**) Cube + diamond. (**f**) Hexagon honeycomb. (**g**) Topology optimization

5.3 Design of a sandwich panel under distributed load

In this section, another advantage of the proposed method, which is the ability of maintaining unique unit cell behaviors during the optimization, is demonstrated. In this design problem, a panel under a distributed load is designed with the re-entrant honeycomb structure with negative Poisson's ratio, an example of a unique property of cellular structures. Figure 13(a) depicts the loading condition and the dimensions of the design problem. The parameterization and pre-analyzed scaling law are presented in Fig. 13(b) and Fig. 13(c), respectively. In this work, the relative density range in the macroscale structural optimization was set to be in the range of 0.2~0.6 to maintain the negative Poisson's ratio. Additionally, the total volume fraction of the structure was set as 0.4. For the microscale structural optimization, an inappropriate set of design parameter constraints could also cause a designed structure to lose its negative Poisson's ratio behavior. In this design example, the microscale wall thickness range was set between 0.2 and approximately 0.6 (mm), and the blending parameter range from 4 to approximately 24. The global blending parameter was set to 4 to ensure smooth interchanges between unit cells. The input data and design constraints are summarized in Table 5.

Figure 14 demonstrates the design result. The total stiffness of the structure is enhanced by 23.91% with a reduction in structural compliance from 55,919.2 to 42,550.5, compared with the non-optimized microstructure FGCS. Moreover, from Fig. 15, the negative Poisson's ratio characteristic of the re-entrant honeycomb structure, illustrated by the C_{12} component in the effective compliance matrix, is maintained during the optimization.

5.4 Applications on infill design of engineering parts

To further prove the practicality of the proposed method, two practical design examples were conducted. The infill design problem of a piston rod under static load was considered in the first example, while a curved sandwich panel design was demonstrated in the second example. Both structures are commonly used in automotive and aerospace industries. Boundary

Table 2 Unit cell stiffness comparison for the single unit cell optimization problem

No.	Unit cell	Unit cell stiffness			
		1	2	3	4
1	Cube	1138.87	77.58	945.60	825.38
2	Diagonal	533.66	344.36	939.75	596.78
3	Diamond	532.77	345.94	958.76	662.76
4	Cube + diagonal	854.00	264.92	973.13	704.37
5	Cube + diamond	880.56	272.30	971.45	711.78
6	Hexagon honeycomb	978.82	149.73	876.55	757.76
7	Topology optimization	1245.45	351.00	1005.90	1023.90

Table 3 Time consumption comparison for the single unit cell optimization problem

No.	Unit cell	Time consumption (s)			
		1	2	3	4
1	Cube	52.0	54.2	54.1	46.7
2	Diagonal	57.9	173.1	57.6	50.8
3	Diamond	50.3	95.8	86.8	55.00
4	Cube + diagonal	92.8	32.3	129.9	132.9
5	Cube + diamond	130.1	117.6	128.7	110.4
6	Hexagon honeycomb	150.2	27.1	59.6	170.7
7	Topology optimization	155.4	156.2	146.8	237.2

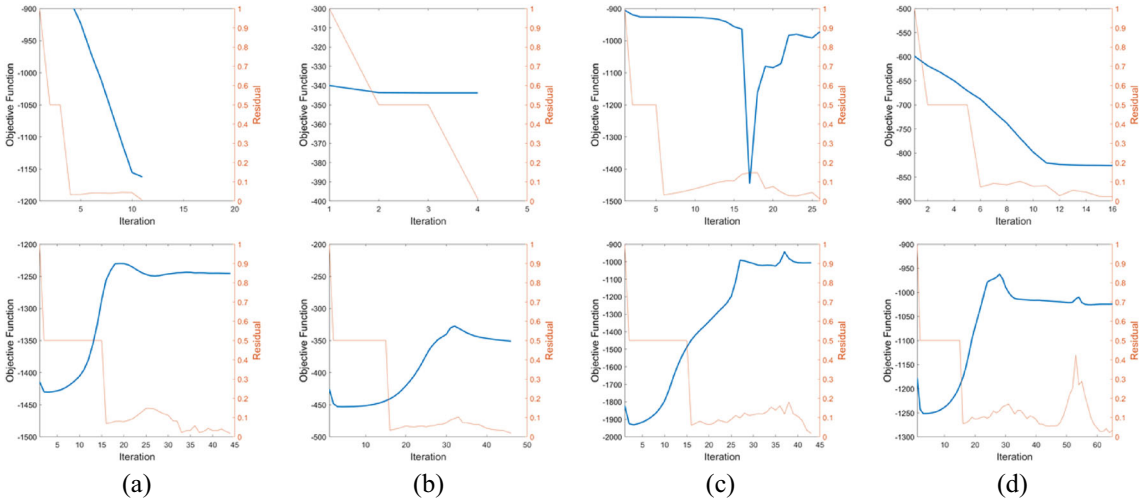

Fig. 8 Convergence history of the (top) best design result by the proposed method and (bottom) topology optimization. (**a**) Strain case 1. (**b**) Strain case 2. (**c**) Strain case 3. (**d**) Strain case 4

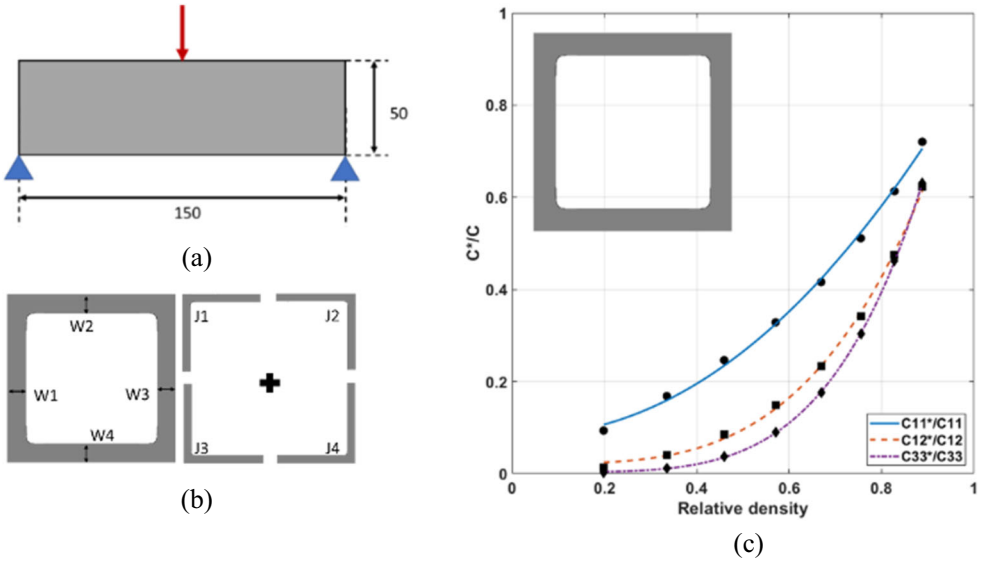

Fig. 9 (**a**) Three-point bending beam design problem. (**b**) Selected unit cell parameterization. (**c**) Pre-analyzed scaling law

Table 4 Design input parameters for the conforming three-point bending beam design problem

Scale	Parameters	Values
Macroscale	Unit cell size (mm)	5
	Scaling law	
	C^*_{11}/C_{11}	$0.85\rho_r^{2.25} + 0.075$
	C^*_{12}/C_{12}	$0.94\rho_r^{3.88} + 0.023$
	C^*_{33}/C_{33}	$1.05\rho_r^{4.52} + 0.002$
	Relative density range	0.3–0.8
	Volume fraction	0.55
Microscale	Grid resolution	50 × 50
	Wall thickness range (mm)	0.15–2.0
	Blending range	2–12

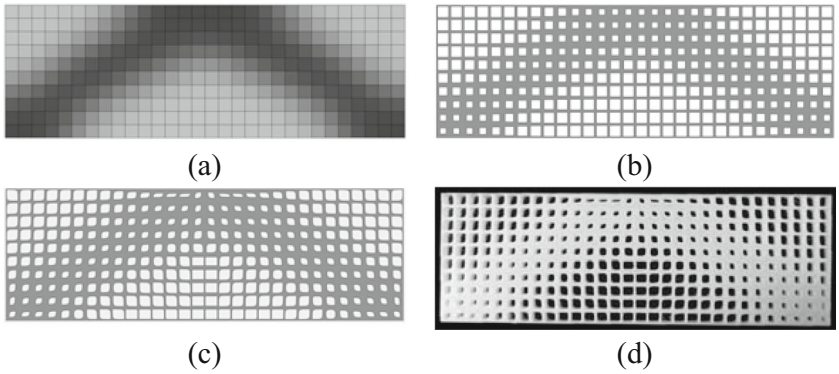

Fig. 10 Design results. (**a**) Density distribution map. (**b**) Non-optimized microstructure. (**c**) Optimized microstructure. (**d**) Fabricated part

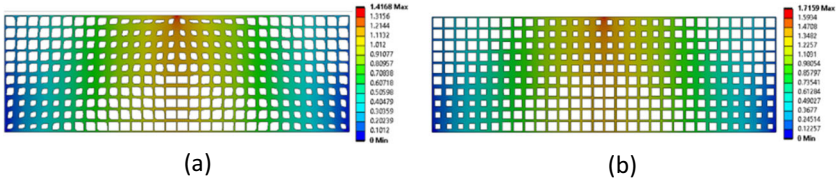

Fig. 11 Nodal displacement comparison of two designs. (**a**) Optimized microstructure. (**b**) Non-optimized microstructure

conditions and design domains in two cases are illustrated in Fig. 16, whereas design input settings are given in Table 6.

Figures 17 and 18 show the results of two cases, including density maps, synthesized structures, and three-dimensional visualizations of final designs. Results from both design cases show enhancements in structural performance, 14.5% for the piston rod case (from 1758.3 to 1510.9) and 24.1% for the curvy sandwich plate case (from 86,209.1 to 65,453.5). This result proved the practicality of the proposed method.

5.5 Discussion

As demonstrated above, the proposed method is capable of deriving comparable optimal solution for structural designs with lower computation cost in comparison with topology optimization. Due to this ability, the proposed method is fit within the context of multiscale structural optimization. In fact, the structural optimization with explicit parameters has gained increased attention due to its practical characteristic (Guo et al. 2014; Liu et al. 2018a; Zhang et al. 2016; Noël and Duysinx 2016; Van Miegroet and Duysinx 2007). However, success of parametric shape optimization usually depends on the effectiveness of shape modeling. In this work, with the joint-based modeling, adequate design freedom is achieved since all the wall thickness and blending parameters at cellular joints are included. As a result, the design degree of freedom is still sufficient to achieve a remarkable enhancement in structural performance, even though the design process is inherently less flexible than that of topology optimization.

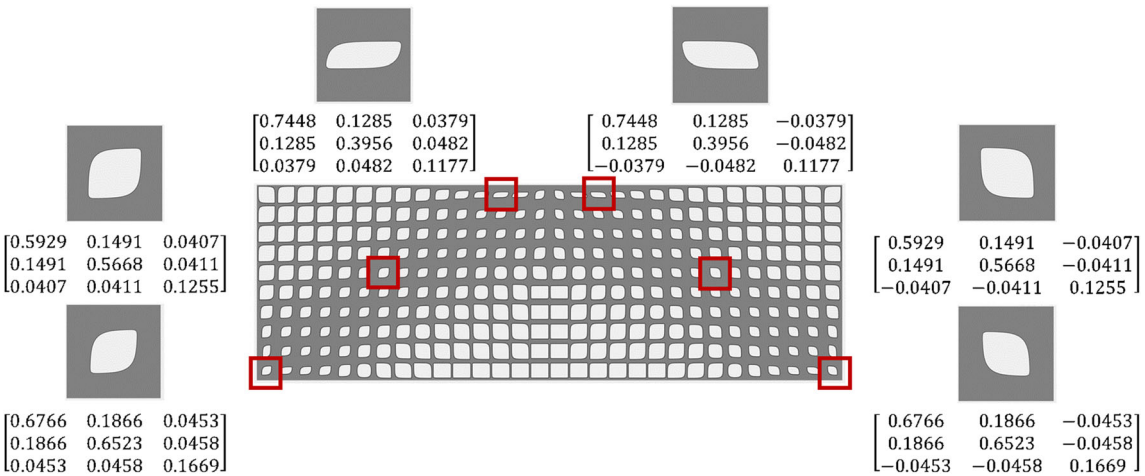

Fig. 12 The designed structure with unit cells having intentional anisotropic elastic properties

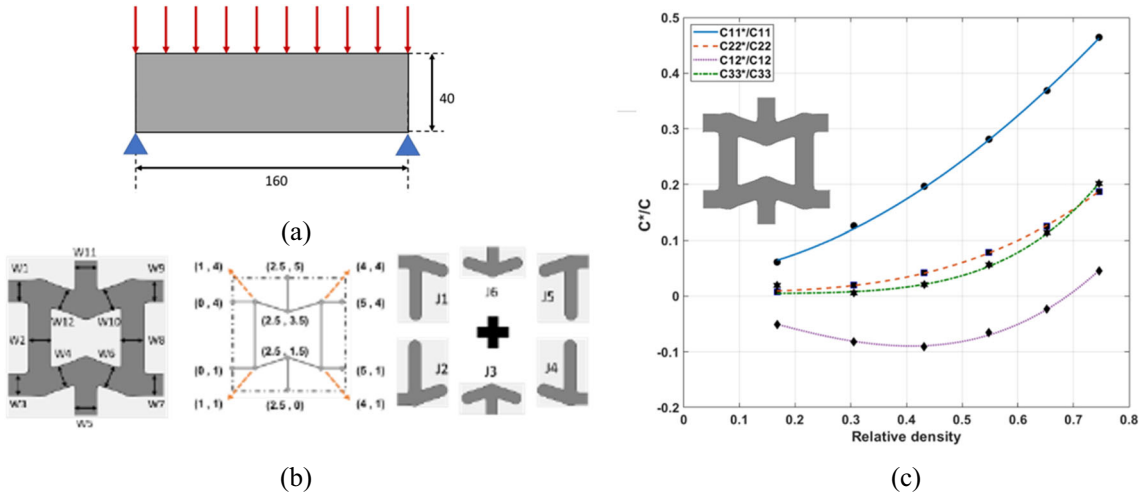

Fig. 13 (**a**) Panel under distributed load design problem. (**b**) Parameterization of re-entrant honeycomb structure. (**c**) Pre-analyzed scaling law of re-entrant honeycomb structure

Table 5 Input parameter for panel under distributed load design problem

Scale	Parameters	Values
Macroscale	Unit cell size (mm)	5
	Scaling law	
	C^*_{11}/C_{11}	$0.73\rho_r^{1.81} + 0.036$
	C^*_{22}/C_{22}	$0.44\rho_r^{3.07} + 0.008$
	C^*_{12}/C_{12}	$0.90\rho_r^3 - 0.21\rho_r^2 - 0.28\rho_r - 0.002$
	C^*_{33}/C_{33}	$0.75\rho_r^{4.54} + 0.005$
	Relative density range	0.2–0.6
	Volume fraction	0.4
Microscale	Grid resolution	50 × 50
	Wall thickness range (mm)	0.2–0.6
	Blending range	4–24

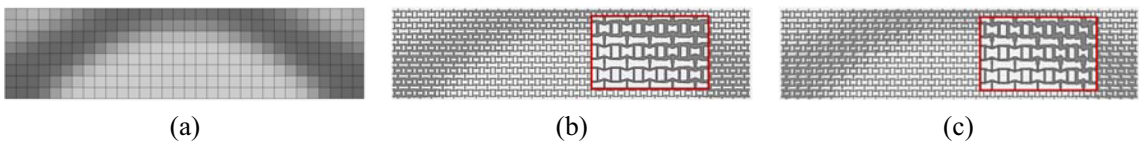

Fig. 14 Panel design result. (**a**) Density map. (**b**) Non-optimized microstructure. (**c**) Optimized microstructure

The experimental results also proved the contribution of the proposed method in FGCS design. As most solutions of FGCS design stop at mapping the optimal density distribution results to geometric parameters of cellular unit cells, the proposed method adds more value with unit cell customization ability, thereby further enhancing the structural performance.

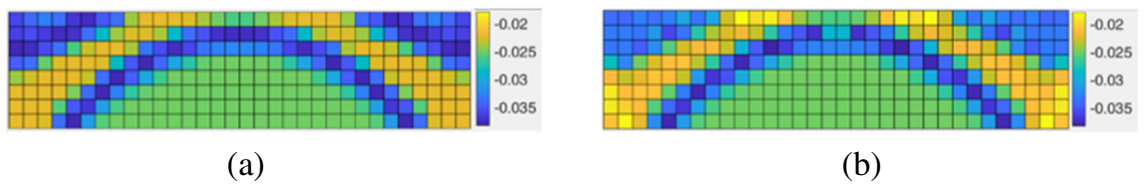

Fig. 15 Plot of C_{12} components of the effective elastic tensor for each unit cell. (**a**) Non-optimized microstructure. (**b**) Optimized microstructure

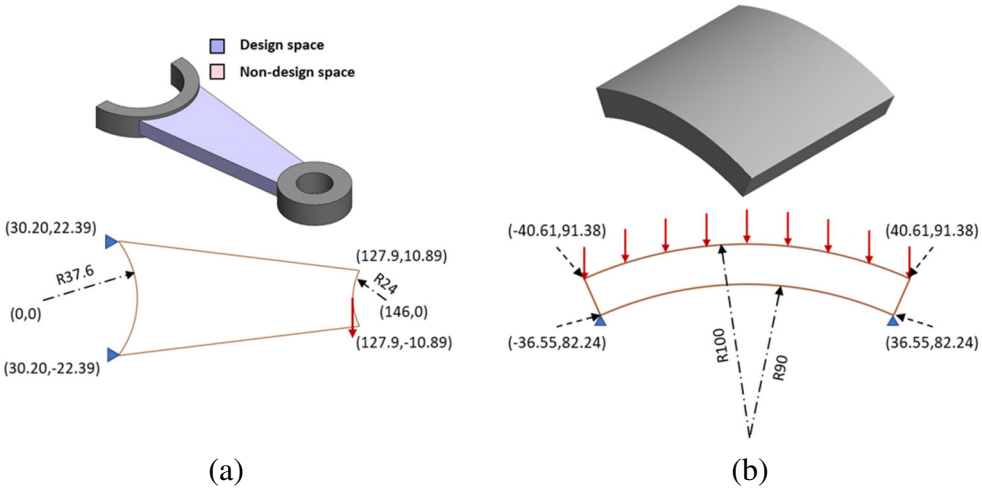

Fig. 16 Design problem for 3D applications. (**a**) Piston rod under static loading. (**b**) Curved sandwich plate under distributed loading

Table 6 Design input for two engineering parts design examples

Parameters	Piston rod	Curvy sandwich plate
Unit cell size (mm)	5	5
Unit cell geometry	Hexagon honeycomb	Re-entrant honeycomb
Relative density range	0.3–0.7	0.2–0.6
Volume fraction	0.5	0.4
Wall thickness range (mm)	0.3–1.0	0.2–0.6
Blending range	4–24	4–24

This is valuable in the research for FGCS design which have been gaining attention due to their better robustness and buckling resistance in comparison with structures designed only by topology optimization (Wu et al. 2018).

Finally, in addition to effortlessly maintaining the unique behavior, the proposed method could derive multifunctional structures without performing multi-objective optimization or adding additional constraints compared to other methods (Geoffroy-Donders et al. 2020; Jiang et al. 2021). This characteristic reduced the complexity of the design problem and made the proposed method more practical. Moreover, one could extend the proposed method by optimally designing cellular unit cell for multifunctional requirement instead of selecting available ones from libraries. Nevertheless, a more general method to efficiently model cellular structure designed by optimization is required to apply the proposed method. This issue will be addressed in a future work.

6 Conclusion

In this work, a level-set-description-based method for multiscale design of FGCSs was proposed. The utilization of implicit blending and joint-based modeling prompts an

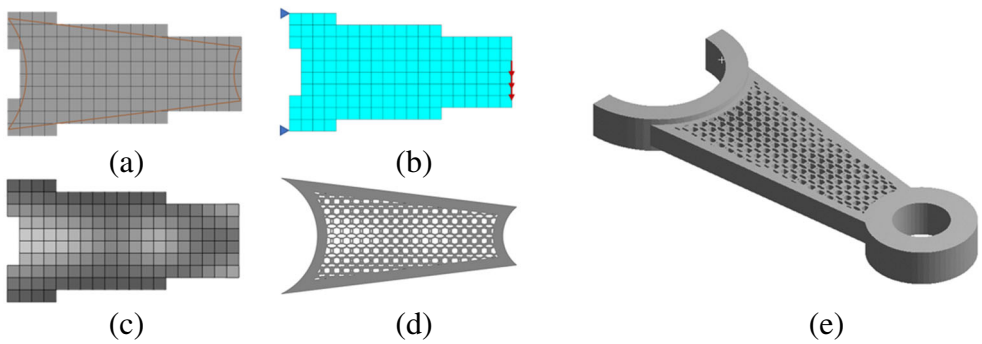

Fig. 17 Piston rod design. (**a**) Design domain tessellation. (**b**) Transferred load applications. (**c**) Optimal density map. (**d**) Reconstructed cellular structure. (**e**) 3D model

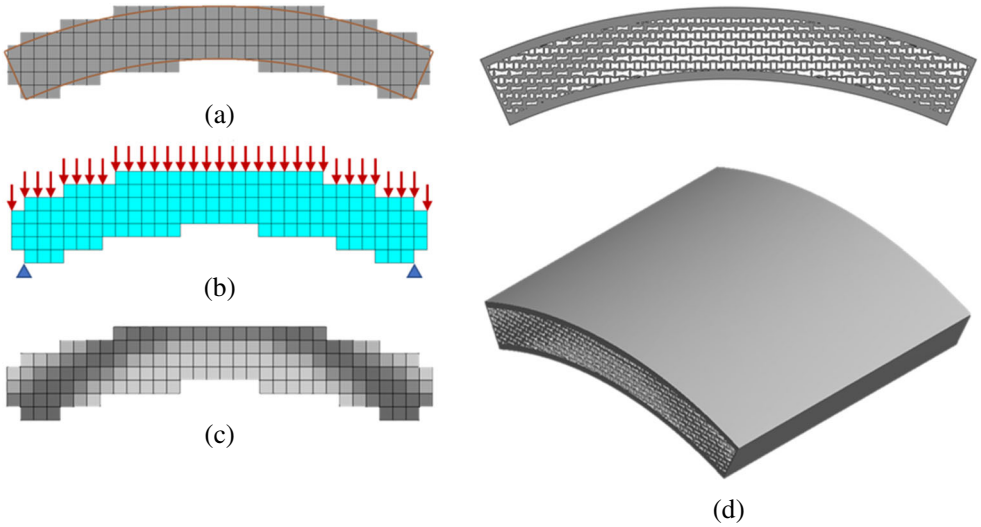

Fig. 18 Curvy sandwich plate design. (**a**) Design domain tessellation. (**b**) Transferred load applications. (**c**) Optimal density map. (**d**) Reconstructed cellular structure and 3D model

efficient structural optimization with enhanced design freedom and relatively low computation cost compared with topology-optimization-based approaches. In addition, two examples of design problems, a three-point bending beam and a sandwich panel under distributed load, were conducted to demonstrate the application in multiscale structural optimization. Moreover, the applicability of the proposed method in practical design problems was validated with two 3D design examples commonly found in automotive and aerospace industries. In all examples, the proposed method remarkably enhanced the structural performance compared to that of the single-scale design approach with non-optimized microstructures. The value of the design process was further increased by its ability to maintain unique behaviors of the pre-selected unit cells during optimization. The proposed approach shows strong promise in the application of concurrent structural optimization, which currently has relied primarily on topology optimization, due to its simplicity and ability to enhance structural performance. In the future, an extension of the proposed approach to more practical design problems, including dynamic loading conditions, stress constraint inclusion, and energy absorption, is intended to be conducted.

Funding This research was supported by the National Research Foundation of Korea (NRF) grant funded by the Korea government (MSIT) (No. 2019R1A2C1002010).

Compliance with ethical standards

Conflict of interest The authors declare that they have no conflict of interest.

Replication of results Sufficient information is presented within the manuscript equipping readers with the tools to replicate the results. Furthermore, computer codes and numerical data needed to reproduce design results and figures in the paper can be accessed by contacting the corresponding author.

References

Allaire G, Jouve F, Toader AM (2004) Structural optimization using sensitivity analysis and a level-set method. J Comput Phys 194(1): 363–393. https://doi.org/10.1016/j.jcp.2003.09.032

Alzahrani M, Choi SK, Rosen DW (2015) Design of truss-like cellular structures using relative density mapping method. Mater Des 85: 349–360. https://doi.org/10.1016/j.matdes.2015.06.180

Cheng L, Zhang P, Biyikli E, Bai JX, Robbins J, To A (2017) Efficient design optimization of variable-density cellular structures for additive manufacturing: theory and experimental validation. Rapid Prototyp J 23(4):660–677. https://doi.org/10.1108/Rpj-04-2016-0069

Fryazinov O, Vilbrandt T, Pasko A (2013) Multi-scale space-variant FRep cellular structures. Comput Aided Des 45(1):26–34. https://doi.org/10.1016/j.cad.2011.09.007

Fu JJ, Li H, Gao L, Xiao M (2019) Design of shell-infill structures by a multiscale level set topology optimization method. Comput Struct 212:162–172. https://doi.org/10.1016/j.compstruc.2018.10.006

Geoffroy-Donders P, Allaire G, Michailidis G, Pantz O (2020) Coupled optimization of macroscopic structures and lattice infill. Int J Numer Methods Eng. https://doi.org/10.1002/nme.6392

Guo X, Zhang WS, Zhong WL (2014) Doing topology optimization explicitly and geometrically-a new moving morphable components based framework. Journal of Applied Mechanics-Transactions of the Asme 81(8):081009. https://doi.org/10.1115/1.4027609

Jiang L, Gu XD, Chen SK (2021) Generative design of bionic structures via concurrent multiscale topology optimization and conformal geometry method. J Mech Des 143(1):1–29. https://doi.org/10.1115/1.4047345

Li DW, Liao WH, Dai N, Dong GY, Tang YL, Xie YM (2018) Optimal design and modeling of gyroid-based functionally graded cellular structures for additive manufacturing. Comput Aided Des 104:87–99. https://doi.org/10.1016/j.cad.2018.06.003

Li DW, Liao WH, Dai N, Xie YM (2020) Anisotropic design and optimization of conformal gradient lattice structures Computer-Aided Design:119. https://doi.org/10.1016/j.cad.2019.102787

Liu C, Zhu YC, Sun Z, Li DD, Du ZL, Zhang WS et al (2018a) An efficient moving morphable component (MMC)-based approach for multi-resolution topology optimization. Struct Multidiscip Optim 58(6):2455–2479. https://doi.org/10.1007/s00158-018-2114-0

Liu JK, Gaynor AT, Chen SK, Kang Z, Suresh K, Takezawa A et al (2018b) Current and future trends in topology optimization for additive manufacturing. Struct Multidiscip Optim 57(6):2457–2483. https://doi.org/10.1007/s00158-018-1994-3

Nguyen CHP, Kim Y, Choi Y (2019) Design for additive manufacturing of functionally graded lattice structures: a design method with process induced anisotropy consideration. International Journal of Precision Engineering and Manufacturing-Green Technology 8(1): 29–45. https://doi.org/10.1007/s40684-019-00173-7

Noël L, Duysinx P (2016) Shape optimization of microstructural designs subject to local stress constraints within an XFEM-level set framework. Struct Multidiscip Optim 55(6):2323–2338. https://doi.org/10.1007/s00158-016-1642-8

Panetta J, Rahimian A, Zorin D (2017) Worst-case stress relief for microstructures. ACM Trans Graph 36(4):1–16. https://doi.org/10.1145/3072959.3073649

Sivapuram R, Dunning PD, Kim HA (2016) Simultaneous material and structural optimization by multiscale topology optimization. Struct Multidiscip Optim 54(5):1267–1281. https://doi.org/10.1007/s00158-016-1519-x

Song YZ, Yang ZW, Liu Y, Deng JS (2018) Function representation based slicer for 3D printing. Computer Aided Geometric Design 62:276–293. https://doi.org/10.1016/j.cagd.2018.03.012

Steuben JC, Iliopoulos AP, Michopoulos JG (2016) Implicit slicing for functionally tailored additive manufacturing. Comput Aided Des 77: 107–119. https://doi.org/10.1016/j.cad.2016.04.003

Svanberg K (1987) The method of moving asymptotes - a new method for structural optimization. Int J Numer Methods Eng 24(2):359–373. https://doi.org/10.1002/nme.1620240207

Tang YL, Zhao YF (2018) Multifunctional design of heterogeneous cellular structures. Struct Multidiscip Optim 58(3):1121–1138. https://doi.org/10.1007/s00158-018-1956-9

Tang YL, Kurtz A, Zhao YF (2015) Bidirectional evolutionary structural optimization (BESO) based design method for lattice structure to be fabricated by additive manufacturing. Comput Aided Des 69:91–101. https://doi.org/10.1016/j.cad.2015.06.001

Van Miegroet L, Duysinx P (2007) Stress concentration minimization of 2D filets using X-FEM and level set description. Struct Multidiscip Optim 33(4-5):425–438. https://doi.org/10.1007/s00158-006-0091-1

Velho, L., Gomes, J., & Figueiredo, L. H. d. (2002). Implicit objects in computer graphics. Springer Verlag New York.

Wang MY, Wang XM, Guo DM (2003) A level set method for structural topology optimization. Comput Methods Appl Mech Eng 192(1-2): 227–246. https://doi.org/10.1016/S0045-7825(02)00559-5

Wang YQ, Chen FF, Wang MY (2017) Concurrent design with connectable graded microstructures. Comput Methods Appl Mech Eng 317: 84–101. https://doi.org/10.1016/j.cma.2016.12.007

Wang YQ, Zhang L, Daynes S, Zhang HY, Feih S, Wang MY (2018) Design of graded lattice structure with optimized mesostructures for additive manufacturing. Mater Des 142:114–123. https://doi.org/10.1016/j.matdes.2018.01.011

Wu J, Aage N, Westermann R, Sigmund O (2018) Infill optimization for additive manufacturing-approaching bone-like porous structures. IEEE Trans Vis Comput Graph 24(2):1127–1140. https://doi.org/10.1109/TVCG.2017.2655523

Wu ZJ, Xia L, Wang ST, Shi TL (2019) Topology optimization of hierarchical lattice structures with substructuring. Comput Methods Appl Mech Eng 345:602–617. https://doi.org/10.1016/j.cma.2018.11.003

Xia L (2016a) Appendix - Design of extreme materials in Matlab. In: Multiscale Structural Topology Optimization. Elsevier, pp 119–143. https://doi.org/10.1016/B978-1-78548-100-0.50010-0

Xia L (2016b) Simultaneous topology optimization of structure and materials. In: Xia L (ed) Multiscale Structural Topology Optimization (pp. 67-88). Elsevier. https://doi.org/10.1016/b978-1-78548-100-0.50004-5

Xia L (2016c) Topology optimization framework for multiscale nonlinear structures. In: Xia L (ed) Multiscale Structural Topology Optimization (pp. 1-19). Elsevier. https://doi.org/10.1016/b978-1-78548-100-0.50001-x

Zhang P, Toman J, Yu Y, Biyikli E, Kirca M, Chmielus M et al (2015) Efficient design-optimization of variable-density hexagonal cellular structure by additive manufacturing: theory and validation. Journal of Manufacturing Science and Engineering-Transactions of the Asme 137(2):021004–021004-8. https://doi.org/10.1115/1.4028724

Zhang WS, Yuan J, Zhang J, Guo X (2016) A new topology optimization approach based on moving morphable components (MMC) and the ersatz material model. Struct Multidiscip Optim 53(6):1243–1260. https://doi.org/10.1007/s00158-015-1372-3